Ultrasound in Med. & Biol., Vol. 37, No. 4, pp. 539–548, 2011

0301-5629/$ - see front matter

ELSEVIER

doi:10.1016/j.ultrasmedbio.2011.01.006

● *Original Contribution*

COMPUTER-AIDED DIAGNOSIS FOR THE CLASSIFICATION OF BREAST MASSES IN AUTOMATED WHOLE BREAST ULTRASOUND IMAGES

Woo Kyung Moon,* Yi-Wei Shen,† Chiun-Sheng Huang,‡ Li-Ren Chiang,† and Ruey-Feng Chang†§

*Department of Diagnostic Radiology, Seoul National University Hospital, Korea; †Department of Computer Science and Information Engineering, National Taiwan University, Taipei, Taiwan; ‡Department of Surgery, National Taiwan University Hospital, Taipei, Taiwan; and §Graduate Institute of Biomedical Electronics and Bioinformatics, National Taiwan University, Taipei, Taiwan

(*Received* 19 *August* 2010; *revised* 23 *November* 2010; *in final form* 7 *January* 2011)

Abstract—New automated whole breast ultrasound (ABUS) machines have recently been developed and the ultrasound (US) volume dataset of the whole breast can be acquired in a standard manner. The purpose of this study was to develop a novel computer-aided diagnosis system for classification of breast masses in ABUS images. One hundred forty-seven cases (76 benign and 71 malignant breast masses) were obtained by a commercially available ABUS system. Because the distance of neighboring slices in ABUS images is fixed and small, these continuous slices were used for reconstruction as three-dimensional (3-D) US images. The 3-D tumor contour was segmented using the level-set segmentation method. Then, the 3-D features, including the texture, shape and ellipsoid fitting were extracted based on the segmented 3-D tumor contour to classify benign and malignant tumors based on the logistic regression model. The Student's *t* test, Mann-Whitney U test and receiver operating characteristic (ROC) curve analysis were used for statistical analysis. From the *Az* values of ROC curves, the shape features (0.9138) are better than the texture features (0.8603) and the ellipsoid fitting features (0.8496) for classification. The difference was significant between shape and ellipsoid fitting features ($p = 0.0382$). However, combination of ellipsoid fitting features and shape features can achieve a best performance with accuracy of 85.0% (125/147), sensitivity of 84.5% (60/71), specificity of 85.5% (65/76) and the area under the ROC curve *Az* of 0.9466. The results showed that ABUS images could be used for computer-aided feature extraction and classification of breast tumors. (E-mail: rfchang@csie.ntu.edu.tw) **© 2011 World Federation for Ultrasound in Medicine & Biology.**

Key Words: **Breast cancer, Automated whole breast ultrasound, Computer-aided diagnosis, Ellipsoid fitting, Logistic regression model.**

INTRODUCTION

The detection accuracy of screening mammography for tumors is severely limited in women with dense breasts (Gordon and Goldenberg 1995; Kolb et al. 1998; Berg et al. 2008; Nothacker et al. 2009; Izumori et al. 2010) and the supplemental screening ultrasound (US) has the potential to detect early breast cancers not seen on mammography and to further reduce mortality (Kolb et al. 2002; Crystal et al. 2003; Leconte et al. 2003; Nothacker et al. 2009). In the results of the first-year screen in ACRIN 6666 (Berg et al. 2008), adding the screening US to mammography will yield an additional 1.1 ∼ 7.2 cancers per 1000 high-risk women.

However, screening using a conventional hand-held probe is operator dependent and, thus, some areas of the breast may not be scanned (Ikedo et al. 2007). In manual US, a breast tumor should be immediately characterized during the examination and a second evaluation of the tumors is difficult due to the lack of standardization of US documentation (Kotsianos-Hermle et al. 2009). Moreover, the cost-effectiveness of manual US for mass screening remains to be evaluated and the time to perform bilateral screening US, at a median of 19 min, is still problematic (Berg et al. 2008). Hence, several automated breast ultrasound (ABUS) machines have been developed and the US volume dataset of the whole breast can be acquired in a standard manner. The Sonociné system (Sonociné Inc., Reno, NV, USA) uses a computer-guided

Address correspondence to: Ruey-Feng Chang, Department of Computer Science and Information Engineering, National Taiwan University, Taipei, Taiwan 10617, R.O.C. E-mail: rfchang@csie.ntu.edu.tw

arm to automatically manipulate a conventional US probe to perform and record an entire breast examination (Kelly et al. 2010). In the study by Kelly et al. (Kelly et al. 2010), the ABUS resulted in significant improvement of cancer detection, compared with mammography alone. Using ABUS with mammography, breast cancer detection doubled from 23 to 46 in 6425 studies. Some ABUS systems use larger probes to scan a larger area. In the Aloka ABUS system (Aloka Inc., Tokyo, Japan), the probe width is 6 cm and only three passes are required to cover one breast (Ikedo et al. 2007; Chang et al. 2010). Patients are in the prone position, different from the conventional supine position. In the U-systems (U-systems Inc., San Jose, CA, USA) and Siemens (Siemens Healthcare, Erlangen, Germany) ABUS systems, the probe width is 15.4 cm and patients are in the normal supine position. In this article, the computer-aided diagnosis system (CAD) is based on the U-systems ABUS machine.

Most of the CAD systems for breast US are based on two-dimensional (2-D) US images (Chen et al. 1999; Shen et al. 2007a; 2007b). Although the 2-D CAD method could be applied for ABUS images of tumors, the three-dimensional (3-D) CAD method could have better diagnostic performance due to making good use of the 3-D information. In the study of Shen et al., the tumor contours drawn by physicians for 2-D US images were used to extract several useful features (Shen et al. 2007a, 2007b).

The purpose of this study was to develop a novel CAD system for classification of breast masses in ABUS images. In this study, a 3-D automatic segmentation method was proposed for segmentation of the tumor and the 3-D texture and morphology features were then used for classification of tumors in ABUS images.

MATERIALS AND METHODS

Patients and lesion characteristics

Informed consent was collected from all of the involved patients and was ratified by the local ethics committee. Data used in this article were collected between October 2007 and January 2008 and consisted of 147 biopsy-proved lesions (76 benign and 71 malignant masses, size range from 0.2 to 5.3 cm, mean 0.9 $\pm$ 0.4 cm) in 140 women (age range from 20 to 79 years, mean 45 $\pm$ 10 years) for evaluation of the performance of the diagnostic system. Benign lesions included 38 fibrocystic changes, five papillomas and 33 fibroadenomas. Malignant lesions included infiltrating carcinomas in 64 patients and ductal carcinoma in situ (DCIS) in seven patients.

Data acquisition

In this study, data from whole breast US were acquired by the SomoVu ScanStation (U-systems, San Jose, CA, USA). In the SomoVu ScanStation, a 10 MHz linear transducer whose width is 15.4 cm is used to scan the larger breast area simultaneously. Although the SomoVu ScanStation can scan a larger area of the breast automatically, compared with other conventional US machines with shorter transducers, it still cannot scan the whole breast and three to five passes of scanning are necessary for complete scanning of the whole breast.

In each scanning pass, the motor-driven transducer automatically moved on the breast skin and a sequence of 2-D 548 $\times$ 348 slices in 35 $\times$ 76 pixels/cm^2 could be obtained for the scanned breast location. The volumetric data could be reconstructed from these continuous 2-D slices because the distance of neighboring slices is fixed and small. The distance between each slice is 16 pixels/cm in this study. For example, some continuous 2-D slices in an ABUS case and their reconstructed 3-D images are shown in Figure 1a and b.

The proposed CAD method

For diagnosis of a tumor in an ABUS image, the volume-of-interest (VOI) containing the tumor is selected by the user. An automatic segmentation method, the level set method (Sethian 1996, 1999), is applied for extraction of the tumor from the VOI. After segmenting the tumor contour, the diagnosis features could be extracted using the B-mode image and the tumor contour. Two kinds of diagnosis features, texture and morphology, are used in this article. The texture features (Haralick et al. 1973; Haralick 1979; Chen et al. 2007) are included in the B-mode features, while the shape features and the ellipsoid fitting features are included in the morphology features. The proposed system is shown in Figure 2.

Tumor segmentation

Before segmenting the tumor in the 3-D ABUS image, the VOI containing the tumor is manually selected by the user. For example, the selected VOI for the ABUS case in Figure 1 is represented by a bounding box in each view, as shown in Figure 1b, and this selected VOI is shown in Figure 1c and d.

In general, if the segmentation method is directly applied in the original US image, the segmentation result might not be good due to speckle noise. Hence, in this article, the contrast-enhanced gradient image is used as the input of the segmentation method. The contrast of the original US image is enhanced by the sigmoid filter (Suri et al. 2008) at first. To obtain a better gradient magnitude image (Gonzalez et al. 2008), the enhanced image is smoothed by the sigma edge-preserving smoothing filter (Lee 1983). Finally, the sigmoid filter is applied again to obtain the contrast-enhanced gradient image for the gradient magnitude image. After preprocessing, the level set method was applied for segmentation of the tumor

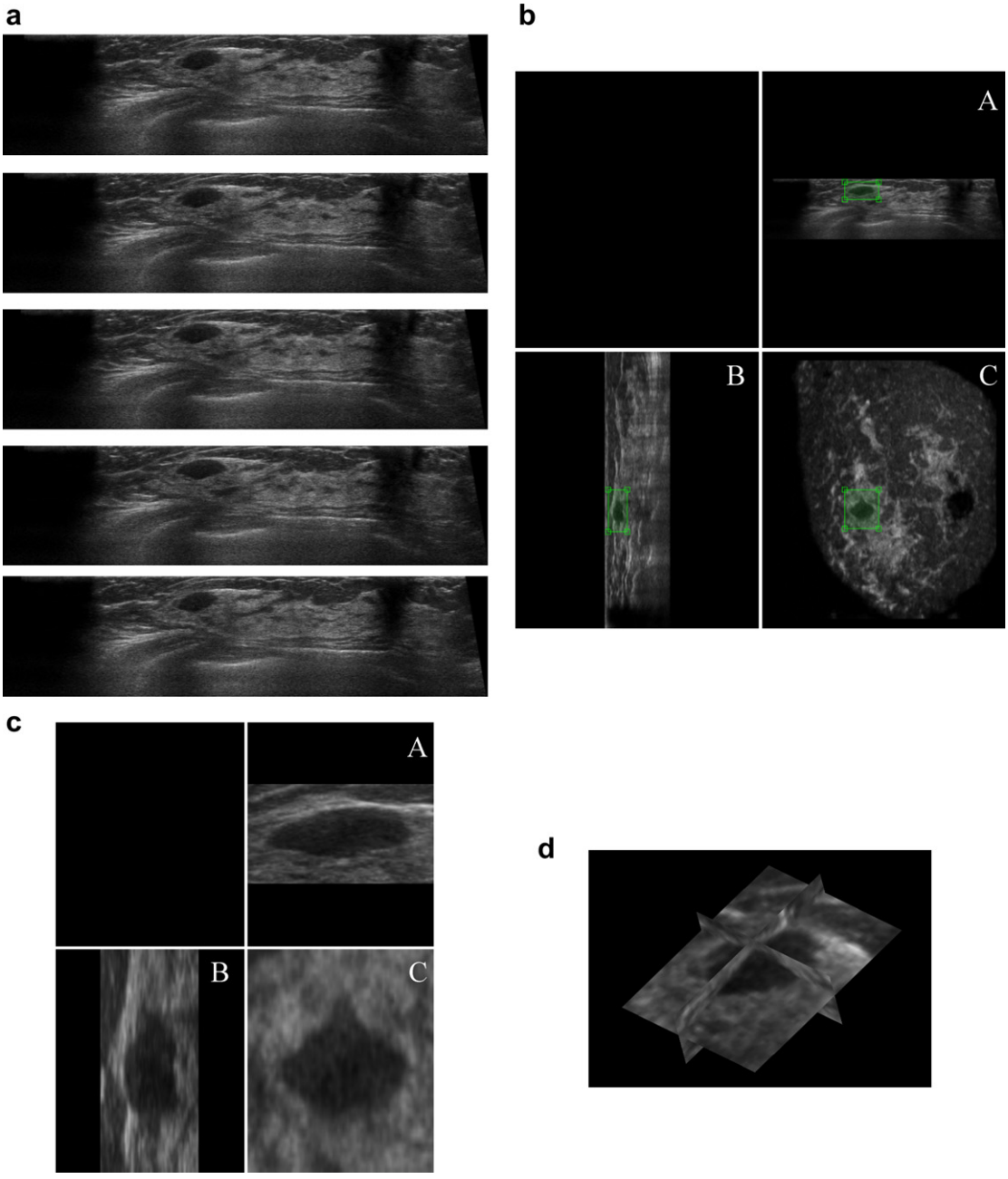

Fig. 1. 3-D automated breast ultrasound (ABUS) images obtained from a 41-year-old woman with a fibroadenoma. (a) Continuous 2-D slices in A view. (b) The reconstructed 3-D image in A, B and C views. The bounding box represents the selected tumor VOI. (c) The VOI in A, B and C views. (d) The VOI in 3-D view.

from the VOI. At first, the operator needs to select the seed points for the level set segmentation and the seed points were used for generation of the initial segmentation. Then, the level set function could iteratively adjust the contour until the level set function was converged. Following application of the level set method to obtain the tumor contour for the contrast-enhanced gradient image, a mathematical morphology closing operation (Gonzalez et al. 2008) is performed to fill the small holes inside the tumor and to make the tumor boundary smoother. An example of segmentation result is shown in Figure 3 and two examples of tumor segmentation in the 3-D view are illustrated in Figure 4.

Feature extraction

Following segmentation, several features are proposed to describe the characteristics of the tumor for diagnosis. These features are categorized into three parts:

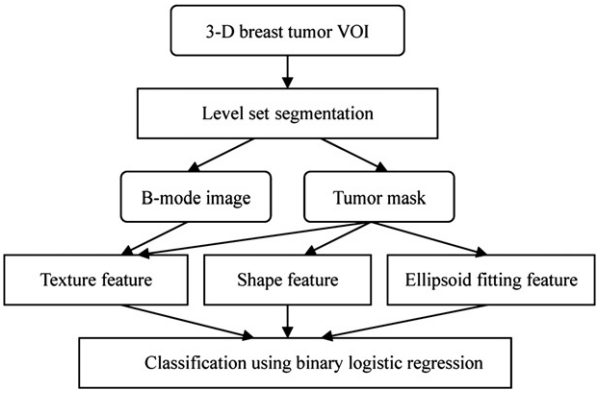

Fig. 2. The system flowchart. The computer-aided classification system is based on texture, shape and ellipsoid fitting features extracted from breast masses in 3-D automated breast ultrasound (ABUS) images.

gray level co-occurrence matrix (GLCM) features, shape features and ellipsoid fitting features. The 2-D images can be well classified using these features (Alvarenga et al. 2007; Shen et al. 2007a, 2007b); however, in 3-D US images they should be defined extensively according to the higher dimension.

The GLCM features (Haralick et al. 1973) are a set of texture features calculated from the co-occurrence matrix G for quantification of the spatial dependence of gray level values. Often used texture-based features extracted from GLCMs include energy (G_1), entropy (G_2), correlation (G_3), inverse difference moment (G_4), inertia (G_5), cluster shade (G_6), cluster prominence (G_7) and Haralick's correlation (G_8) (Haralick et al. 1973).

The proposed shape features include two major categories, the margin and the compactness of volume structure. The radius and spiculation (Meinel et al. 2007) are used to characterize the margin property, while the two compactness definitions of 3-D objects (Bribiesca 2008) are used to measure the relation between surface and volume of tumor. Radius and spiculation (Meinel et al. 2007) are the mean and standard deviations of the distance between tumor center and boundary voxels and both reflect the variation of the tumor boundary. The radius means the average size of the tumor and the spiculation describes the irregularity of the surface. Let the tumor center (x_c, y_c, z_c) be

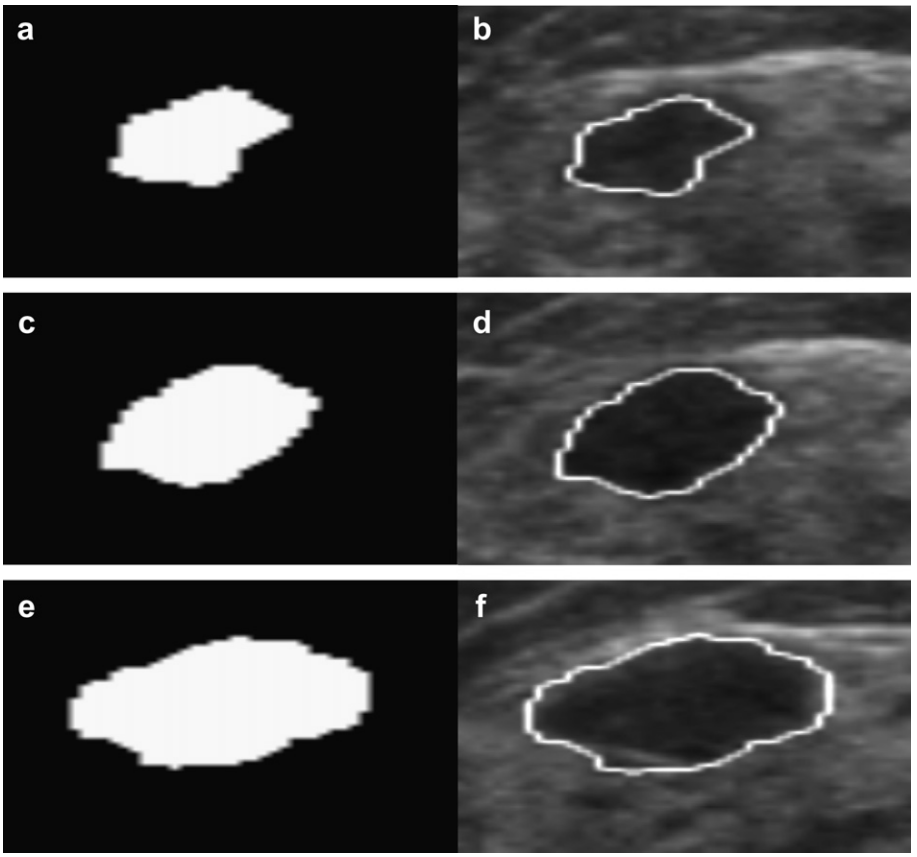

Fig. 3. (a), (c) and (e) The tumor region segmented using the level set method for fibroadenoma (case in Fig. 1). (b), (d) and (f) The segmented tumor contour overlapped in the original image.

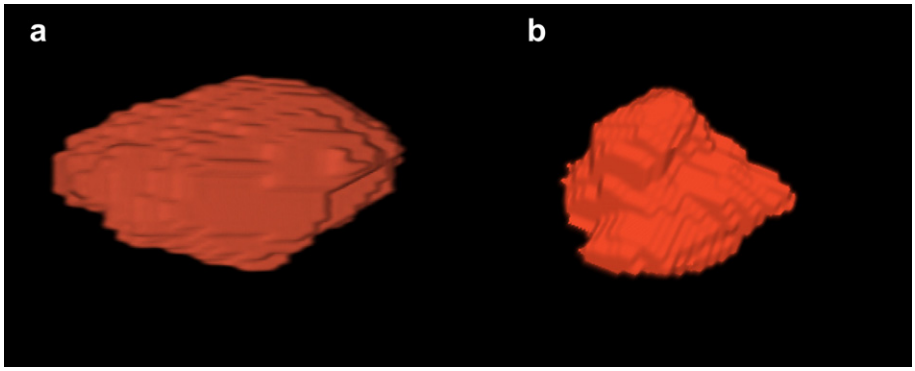

Fig. 4. Results of segmentation in 3-D view. (a) Fibroadenoma (case in Fig. 3) (b) Invasive cancer.

$$x_c=\frac{1}{N}\sum_{i=1}^{N}x_i \ , \ y_c=\frac{1}{N}\sum_{i=1}^{N}y_i \ , \ z_c=\frac{1}{N}\sum_{i=1}^{N}z_i. \quad (1)$$

The radius R and spiculation R_s can then be defined as

$$R=\frac{1}{n_b}\sum_{(i,j,k)\in boundary}\sqrt{(i-x_c)^2+(j-y_c)^2+(k-z_c)^2} \quad (2)$$

$$R_s=\sqrt{\frac{\sum_{x\in boundary}(R_x-R)^2}{n_b-1}} \quad (3)$$

where n_b is the number of boundary voxels. Compactness is a measurement of the connectedness of the parts within an object. In this article, two different definitions of 3-D image compactness, C_1 and C_2, are defined as (Bribiesca 2008)

$$C_1=\frac{36\pi\cdot V^2}{A^3} \quad (4)$$

$$C_2=\frac{n-\frac{A}{6a}}{n-\sqrt[3]{n^2}} \quad (5)$$

where A and V denote the surface area and volume of the tumor, a is the area of one surface of a voxel and n is the number of voxels in the tumor.

In general, benign tumors have a regular shape (close to sphericity); however, malignant tumors have a more irregular shape. Hence, we can use an ellipsoid to fit the tumor. The difference and similarity between the tumor and the fitting ellipsoid model can be measured in many ways and some measurements have been shown to be useful for 2-D US images (Shen et al. 2007a). In this article, the best fit ellipsoid E is obtained by minimizing the distance between the tumor and the built ellipsoid model (Zhu and Poh 1988; Mulchrone and Choudhury 2004).

After construction of the ellipsoid model, several useful 2-D features (Shen et al. 2007a) are extended to the 3-D form features in this article. The axis ratio ER_{axis} is defined as

$$ER_{axis}=\frac{\max\{L_1,L_2,L_3\}}{\min\{L_1,L_2,L_3\}} \quad (6)$$

The surface ratio $ER_{surface}$, which measures the ratio between tumor surface A and ellipsoid surface A_e, is defined as

$$ER_{surface}=\frac{A}{A_e} \quad (7)$$

where the surface area A_e is given by (Ulanovsky and Prohl 2006)

$$A_e=4\pi\left(\frac{L_1^pL_2^p+L_2^pL_3^p+L_3^pL_1^p}{3}\right)^{\frac{1}{p}} \quad (8)$$

L_1, L_2 and L_3 are the lengths of the semi-principal axes and $p = 1.6075$ yields a relative error of at most 1.061%.

The volume covering ratio ER_{and}, which measures the similarity between ellipsoid and the real tumor by the intersection of two objects, is defined as

$$ER_{and}=\frac{volume(v_{tumor}\cap v_e)}{V} \quad (9)$$

where V is the volume of the tumor; v_{tumor} and v_e are the voxel sets of tumor and ellipsoid, respectively. The operator $\cap$ is the intersection of the above two sets.

The number of different regions between the tumor and the ellipsoid are also used in quantification of the tumor. The outside regions denote the tumor region lying outside the ellipsoid and the inside regions denote the ellipsoid region lying outside the tumor.

Figure 5 shows inside and outside regions. The feature EN_{out} is the number of outside regions and the EN_{in} is the number of inside regions. The sum of total regions of inside and outside: $EN_{io}= EN_{in}+EN_{out}$. The

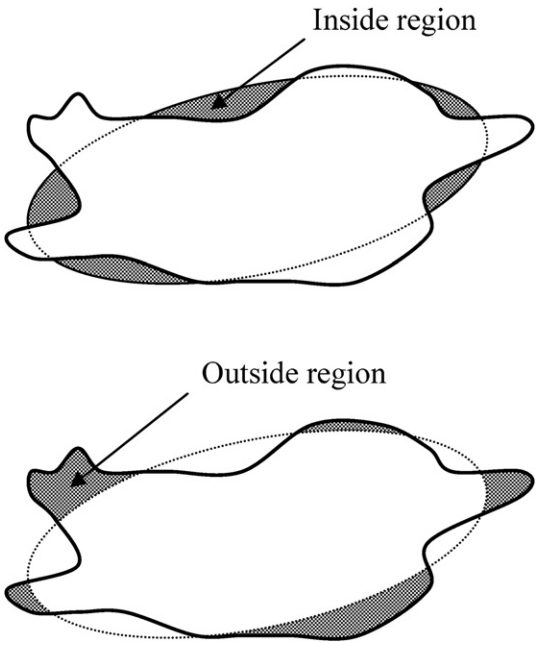

Fig. 5. Inside and outside regions.

orientation feature E_{angle} is the angle between the normal direction of the horizontal plane and the major (longest) axis of the corresponding ellipsoid.

The number of angular parts can reflect how the tumor is diverse from the fitting ellipsoid. The angularity characterizes the protruding level in the outside region and the indenting level in the inside region. For an outside region, its angularity is defined by the maximum angular ratio of the region, which is denoted by a/b: a is the distance of an outside contour point from the tumor center and b is the distance of the corresponding elliptic point from the tumor center. For an inside region, its angularity is defined by the minimum angular ratio of the region, which is denoted by c/d: c is the distance of an inside contour point from the tumor center and d is the distance of the fitting elliptic point from the tumor center, as shown in Figure 6. If an angularity in the outside region is larger than a threshold, or an angularity in the inside region is smaller than a threshold, it is considered as a sharp angularity. The feature EN_{a_out} is the number of sharp angularities in the outside region and the EN_{a_in} is the number of sharp angularities in the inside ones. In this article, the threshold for outside ratio is 1.15 and the threshold for inside ratio is 0.85.

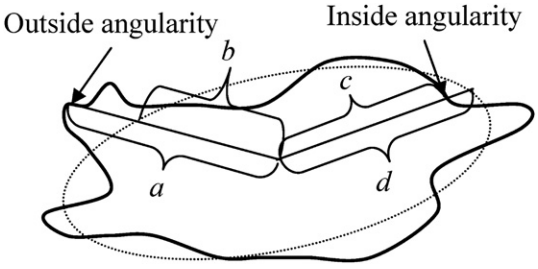

Fig. 6. Inside and outside angular ratios.

Statistical analysis

In the analysis, the Kolmogorov–Smirnov test (Field 2005) was applied to test whether the feature is a normal distribution or not. If the feature was a normal distribution, then the mean values and standard deviation were calculated for the benign and malignant tumors. If the distribution of a feature was not normal, the median value was listed and the Mann-Whitney U test (Field 2005) was used. Differences between the values of the features for the benign and malignant tumors were evaluated with Student's t- test. The relationship between the tumor category and the specified feature can also be assessed by r_{pb} (Behnke 2006). The algorithm relief (Kira and Rendell 1992; Kononenko 1994; Kohavi and John 1997) was also used to estimate the relevance of features.

Diagnostic performance of the binary logistic regression model (Gigliotti 2007; Shen et al. 2007b) based on the proposed features for classification of breast tumors using the leave-one-out cross-validation method (Behnke 2006) was evaluated with accuracy, sensitivity, specificity, positive and negative predictive values and the receiver operating characteristic (ROC) curve analysis by use of the ROCKIT software (C. Metz; University of Chicago, Chicago, IL, USA). Results for the area under the ROC curve (Az) were used as indicators of performance. Statistical analyses other than ROC analysis were performed with statistical software (SPSS, version 16 for Windows; SPSS, Chicago, IL, USA).

RESULTS

Feature analysis

The mean value, standard deviation (SD), median value, p value, point biserial correlation coefficient r_{pb} and relief score of the features are listed in Table 1.

For the p values, the differences of benign and malignant cases for most features, except for the GLCM feature G_1, ellipsoid fitting features ER_{axis}, EN_{in}, EN_{out}, EN_{io}, EN_{a_in} and E_{angle} are statistically significant. For the point biserial correlation coefficient r_{pb} (absolute value > 0.5), the most important features are the shape features C_2 (0.621), R (0.596), C_1 (0.523) and R_s (0.518), ellipsoid fitting feature $ER_{surface}$ (0.528). All of the r_{pb} values of GLCM features are smaller than 0.4. For the relevant relief scores (>0.03), the most important features for differentiation of benign from malignant tumors are the shape features C_2 (0.0607) and C_1 (0.0375), ellipsoid fitting features $ER_{surface}$ (0.0495) and E_{angle} (0.0303). All of the relief scores of GLCM features are smaller than 0.02.

Table 1. Values of the features for benign and malignant tumors

Features		Benign		Malignant				
		Mean ± SD	Median	Mean ± SD	Median	p value	r_{pb}	Relief
GLCM	G_1	$8.62 \times 10^{-4} \pm 2.99 \times 10^{-4}$		$9.52 \times 10^{-4} \pm 2.90 \times 10^{-4}$		0.066	0.152	−0.0013
	G_2	9.61 ± 0.60		9.32 ± 0.21		<0.001	−0.298	0.0172
	G_3		2.61×10^{-3}		3.46×10^{-3}	<0.001	0.241	0.0028
	G_4	0.14 ± 0.02		0.15 ± 0.02		<0.001	0.309	0.0027
	G_5	116.89 ± 41.56		90.04 ± 27.93		<0.001	−0.354	0.0046
	G_6		3.93×10^4		3.20×10^4	0.044	−0.184	0.0095
	G_7		5.77×10^6		4.37×10^6	0.021	−0.194	0.0088
	G_8		4.05×10^7		2.55×10^7	0.004	−0.204	0.0007
Shape	*Volume*		359.47		1546.01	<0.001	0.418	0.0139
	C_1	15.73 ± 3.79		11.45 ± 3.20		<0.001	−0.523	0.0375
	C_2	93.22 ± 1.49		90.37 ± 2.06		<0.001	−0.621	0.0607
	R		4.55		7.75	<0.001	0.596	0.0269
	R_s		0.93		1.73	<0.001	0.518	0.0141
Ellipsoid fitting	ER_{axis}	2.10 ± 0.58		2.11 ± 0.65		0.930	−0.007	0.0150
	$ER_{surface}$		1.70		1.92	<0.001	0.528	0.0495
	ER_{and}	0.86 ± 0.037		0.82 ± 0.05		<0.001	−0.371	0.0270
	EN_{in}		11		9	0.280	−0.088	−0.0082
	EN_{out}		12		14	0.060	0.195	0.0128
	EN_{io}	25.16 ± 9.8		26.87 ± 12.27		0.350	0.078	0.0104
	EN_{a_in}		1		1	0.630	−0.073	0.0100
	EN_{a_out}		3		4	<0.001	0.337	0.0180
	EN_{a_io}		3		5	<0.001	0.295	0.0162
	E_{angle}	0.83 ± 0.48		0.69 ± 0.41		0.055	−0.158	0.0303

GLCM = gray level co-occurrence matrix.

The mean value, standard deviation (SD), median value, p value of Student's t-test or Mann-Whitney U test, point biserial correlation coefficient r_{pb}, and relief score of each feature. The Kolmogorov–Smirnov test is applied to test for a normal distribution. If the distribution of a feature is normal, the mean value and standard deviation are listed and the Student's t-test is used. Otherwise, the median value is listed and the Mann-Whitney U test is used. Before calculations of Student's t-test, the Levene's test had been used for verification of the equality of variances.

Tumor classification

The classification performances of the proposed features using the binary logistic regression model are listed in Table 2 and their ROC curves are shown in Figure 7a. From the five performance indexes, the shape and ellipsoid features are still better than the texture GLCM features. However, from the Az values of ROC curves, the texture GLCM features are better than the ellipsoid fitting features and the shape features is the best set. The performance difference for single feature type in Table 3 shows that only the Az values between shape and ellipsoid fitting have significant differences. After comparison of each feature set, the combined features from two or three sets could be compared. The performance indexes are also listed in Table 2 and their ROC curves are shown in Figure 7b. The p values of five performance indexes and Az value of the ROC curve between different combinations of feature sets are listed in Table 3. The combination of shape and ellipsoid fitting features showed the best performance, with accuracy of 85.0% (125/147), sensitivity of 84.5% (60/71), specificity of 85.5% (65/76) and the area under the ROC curve Az of 0.9466.

DISCUSSION

In our study, the motor-driven transducer with 15.4 cm width automatically moved on the breast skin and a sequence of 2-D 548 × 348 slices in 35 × 76 pixels/cm^2 was obtained for each scanning pass. Volumetric data was then reconstructed from these continuous

Table 2. Result of performance for each feature set

	GLCM	Shape	Ellipsoid fitting	GLCM and shape	GLCM and ellipsoid fitting	Shape and ellipsoid fitting	ALL
Accuracy (%)	75.51 (111/147)	82.31 (121/147)	79.59 (117/147)	80.27 (118/147)	81.63 (120/147)	85.03 (125/147)	82.31 (121/147)
Sensitivity (%)	81.69 (58/71)	84.51 (60/71)	76.06 (54/71)	83.10 (59/71)	84.51 (60/71)	84.51 (60/71)	83.10 (59/71)
Specificity (%)	69.74 (53/76)	80.26 (61/76)	82.89 (63/76)	77.63 (59/76)	78.95 (60/76)	85.53 (65/76)	81.58 (62/76)
PPV (%)	71.60 (58/81)	80.00 (60/75)	80.60 (54/67)	77.63 (59/76)	78.95 (60/76)	84.51 (60/71)	80.82 (59/73)
NPV (%)	80.30 (53/66)	84.72 (61/72)	78.75 (63/80)	83.10 (59/71)	84.51 (60/71)	85.53 (65/76)	83.78 (62/74)
Az	0.8603	0.9138	0.8496	0.9153	0.8915	0.9466	0.9388

GLCM = gray level co-occurrence matrix; PPV = positive predictive value; NPV = negative predictive value.

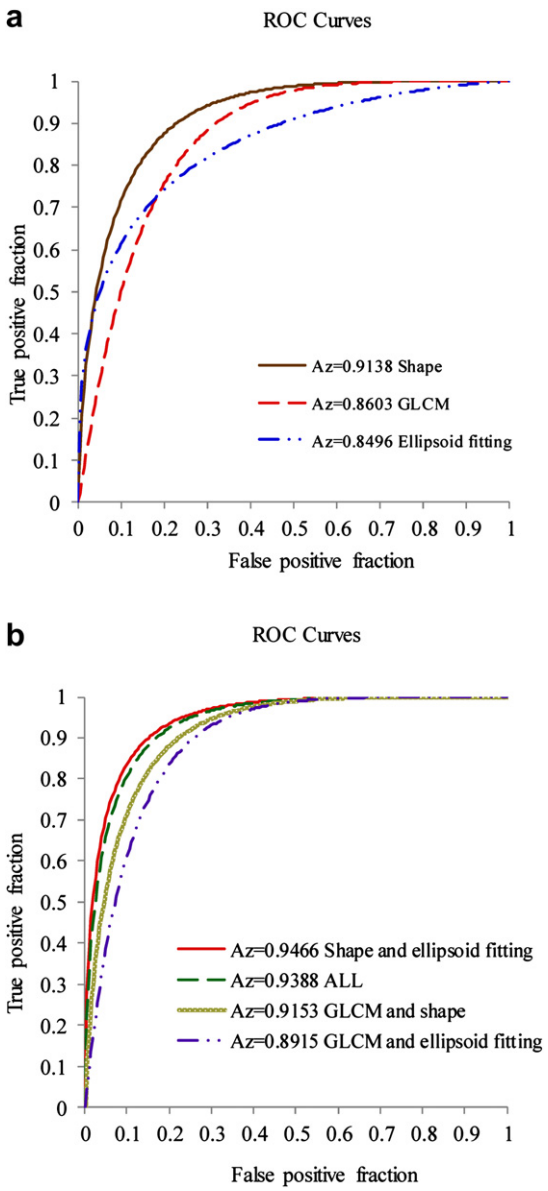

Fig. 7. Receiver operating characteristic (ROC) curves of each feature set. (a) Shape, GLCM and ellipsoid fitting. (b) Combined feature classes. Note that GLCM = gray level co-occurrence matrix.

2-D slices and 3-D images were used for development of a CAD system. In previous CAD studies (Buist et al. 2004; Berg et al. 2008; Chang et al. 2010) for 3-D US images, images were acquired using a small part 3-D probe with a scan width of 4 cm and 20–30° sweep angle. The 2-D scanning planes were produced by movement of the 2-D transducer at regular angular intervals and were arranged in a fanlike geometry. The pixel resolutions of the tumors were from 40.0 pixels/cm to 70.8 pixels/cm. These previous CAD studies were based on texture information. In this ABUS study, not only texture information but also morphology information, such as shape and ellipsoid fitting features, were used. ROC curve analysis showed that the shape features (0.9138) are better than the texture features (0.8603) and the ellipsoid fitting features (0.8496) for classification. However, the combination of shape and ellipsoid fitting features has the best performance for classification of breast tumors, with accuracy of 85.0% (125/147), sensitivity of 84.5% (60/71), specificity of 85.5% (65/76) and the area under the ROC curve Az of 0.9466.

To find morphologic features for diagnosis of breast tumors, the tumor contour needs to be found first. In 2-D US, the operator could easily draw the tumor contour manually or use the interactive line wire extraction (Barrett and Mortensen 1997) for the segmentation. However, in 3-D US, it is difficult to draw the tumor contour for each slice by the above manual methods. In this study, the level set method was used to reduce the operator's effort for the tumor segmentation. The operator only needs to set the seed points inside the tumor and then the level set method could automatically segment the tumor. Compared with the manual drawing tumor contour, the level set method is more convenient and suitable for 3-D US segmentation.

In our study, gray level co-occurrence matrix (GLCM) features, shape features and ellipsoid fitting features were used for classification of breast tumors. The proposed shape features include two major categories, the margin and the compactness of volume structure. The radius and spiculation (Meinel et al. 2007) are used to characterize the margin property, while the two compactness definitions of 3-D objects (Bribiesca 2008) are used to measure the relation between surface and volume of tumor. For ellipsoid fitting features, the difference and similarity between the tumor and the fitting ellipsoid model were measured and used for the feature extraction. These are computed BI-RADS US features of shape, orientation and margin characteristics and the differences of benign and malignant cases are statistically significant for most features. In a benchmark study, Stavros et al. (Stavros et al. 1995) described a US classification model with a reported 99.5% (424 of 426 cases) negative predictive value and 98.4% (123 of 125 cases) sensitivity. The model was based on 20 US features of breast masses, including morphologic descriptors of the shape, margin and texture of a mass and acoustic properties. However, subsequent studies (Rahbar et al. 1999) have shown substantial variability in identification of specific US features, which could yield varying conclusions on the use of US for characterization of solid breast nodules. Interpreter variability in US differentiation of solid breast nodules was emphasized. Although we did not perform a comparison study between the CAD system

Table 3. The p value of five performance indexes using χ^2 test and Az value of the ROC curve using the z-test for different feature classes

	GLCM vs. shape	GLCM vs. ellipsoid fitting	Shape vs. ellipsoid fitting	Shape and ellipsoid fitting vs. GLCM	Shape and ellipsoid fitting vs. shape	Shape and ellipsoid fitting vs. ellipsoid fitting	Shape and ellipsoid fitting vs. all
Accuracy	0.1528	0.4017	0.5525	0.0402*	0.5279	0.2214	0.5279
Sensitivity	0.6543	0.4109	0.2057	0.6543	1.0000	0.2057	0.8198
Specificity	0.1340	0.0564	0.6756	0.0195*	0.3889	0.6564	0.5116
PPV	0.2223	0.2044	0.9289	0.0568	0.4768	0.5447	0.5594
NPV	0.4939	0.8172	0.3429	0.4075	0.8907	0.2703	0.7671
Az	0.0700	0.7836	0.0382*	0.0029*	0.0623	0.0004*	0.1307

GLCM = gray level co-occurrence matrix; ROC = receiver operating characteristic; PPV = positive predictive value; NPV = negative predictive value.

* The difference was statistically significant.

and radiologists in this study, use of the breast US CAD system for tumor characterization was proved with ROC study with or without the aid of a CAD system in other papers (Giger et al. 1999). The US CAD system can provide physicians with a second opinion for tumor characterization and can improve physician performance in the task of differentiating malignant from benign breast lesions on US.

The 3-D power Doppler US is also very useful for diagnosis of breast tumors (Kalmantis et al. 2009). Using the morphologic characteristics of the B-mode image and criteria of the vascular pattern of the color Doppler image, 3-D power Doppler US could identify 49 of 53 cancers, resulting in a sensitivity of 92.4% and a specificity of 86.1% (62/72). In 3-D US CAD studies (Chen et al. 1999; Chang et al. 2007), power Doppler US images were used for extraction of vessel information and the vessel morphology was used for diagnosis of tumors. For the current ABUS, only B-mode images are acquired and vessel morphology could not be used in diagnosis. If power Doppler US images could be obtained in the ABUS machine, then the vessel morphology could be used for improvement of diagnosis in the future.

In conclusion, a 3-D automatic segmentation method was proposed for segmentation of the tumor and computer-aided diagnosis based on the 3-D texture and morphology features were successfully used for classification of the tumor using ABUS images.

Acknowledgments—This work was supported by a grant from the National Science Council of the Republic of China (NSC 99-2221-E-002-136-MY3) and was supported by the Converging Research Center Program through the Ministry of Education, Science and Technology, Republic of Korea (2010K001113).

REFERENCES

Alvarenga AV, Pereira WCA, Infantosi AFC, Azevedo CM. Complexity curve and grey level co-occurrence matrix in the texture evaluation of breast tumor on ultrasound images. Med Phys 2007;34:379–387.

Barrett WA, Mortensen EN. Interactive live-wire boundary extraction. Med Image Anal 1997;1:331–341.

Behnke J. Discovering statistics using spss. Polit Vierteljahr 2006;47: 751–753.

Berg WA, Blume JD, Cormack JB, Mendelson EB, Lehrer D, Bohm-Velez M, Pisano ED, Jong RA, Evans WP, Morton MJ, Mahoney MC, Larsen LH, Barr RG, Farria DM, Marques HS, Boparai K. Combined screening with ultrasound and mammography vs mammography alone in women at elevated risk of breast cancer. JAMA 2008;299:2151–2163.

Bribiesca E. An easy measure of compactness for 2d and 3d shapes. Pattern Recognit 2008;41:543–554.

Buist DS, Porter PL, Lehman C, Taplin SH, White E. Factors contributing to mammography failure in women aged 40–49 years. J Natl Cancer Inst 2004;96:1432–1440.

Chang RF, Chang-Chien KC, Takada E, Huang CS, Chou YH, Kuo CM, Chen JH. Rapid image stitching and computer-aided detection for multipass automated breast ultrasound. Med Phys 2010;37: 2063–2073.

Chang RF, Huang SF, Moon WK, Lee YH, Chen DR. Solid breast masses: Neural network analysis of vascular features at three-dimensional power Doppler USs for benign or malignant classification. Radiology 2007;243:56–62.

Chen DR, Chang RF, Huang YL. Computer-aided diagnosis applied to us of solid breast nodules by using neural networks. Radiology 1999;213:407–412.

Chen W, Giger ML, Li H, Bick U, Newstead GM. Volumetric texture analysis of breast lesions on contrast-enhanced magnetic resonance images. Magn Reson Med 2007;58:562–571.

Crystal P, Strano SD, Shcharynski S, Koretz MJ. Using sonography to screen women with mammographically dense breasts. AJR Am J Roentgenol 2003;181:177–182.

Field A. Discovering statistics using SPSS. 2nd edition. London: SAGE publications; 2005.

Giger ML, Al-Hallaq H, Huo ZM, Moran C, Wolverton DE, Chan CW, Zhong WM. Computerized analysis of lesions in US images of the breast. Acad Radiol 1999;6:665–674.

Gigliotti E. Discovering statistics using SPSS, 2nd edition. J Adv Nurs 2007;58:303.

Gonzalez RC, Woods RE, Masters BR. Digital image processing. Upper Saddle River, New Jersey: Pearson Prentice Hall; 2008.

Gordon PB, Goldenberg SL. Malignant breast masses detected only by ultrasound. A retrospective review. Cancer 1995;76:626–630.

Haralick RM. Statistical and structural approaches to texture. Proc IEEE 1979;67:786–804.

Haralick RM, Shanmuga. K, Dinstein I. Textural features for image classification. IEEE Trans Syst Man Cybern 1973;SMC3:610–621.

Ikedo Y, Fukuoka D, Hara T, Fujita H, Takada E, Endo T, Morita T. Development of a fully automatic scheme for detection of masses in whole breast ultrasound images. Med Phys 2007;34:4378–4388.

Izumori A, Takebe K, Sato A. Ultrasound findings and histological features of ductal carcinoma *in situ* detected by ultrasound examination alone. Breast Cancer 2010;17:136–141.

Kalmantis K, Dimitrakakis C, Koumpis C, Tsigginou A, Papantoniou N, Mesogitis S, Antsaklis A. The contribution of three-dimensional power Doppler imaging in the preoperative assessment of breast tumors: A preliminary report. Obstet Gynecol Int 2009;2009:530579.

Kelly KM, Dean J, Comulada WS, Lee SJ. Breast cancer detection using automated whole breast ultrasound and mammography in radiographically dense breasts. Eur Radiol 2010;20:734–742.

Kira K, Rendell LA. A practical approach to feature selection. Proceedings of the ninth international workshop on Machine learning. Aberdeen, Scotland, United Kingdom: Morgan Kaufmann Publishers Inc; 1992:249–256.

Kohavi R, John GH. Wrappers for feature subset selection. Artif Intell 1997;97:273–324.

Kolb TM, Lichy J, Newhouse JH. Occult cancer in women with dense breasts: Detection with screening US–diagnostic yield and tumor characteristics. Radiology 1998;207:191–199.

Kolb TM, Lichy J, Newhouse JH. Comparison of the performance of screening mammography, physical examination, and breast us and evaluation of factors that influence them: An analysis of 27,825 patient evaluations. Radiology 2002;225:165–175.

Kononenko I. Estimating attributes: Analysis and extensions of relief. Proceedings of the European conference on machine learning on Machine Learning. Catania, Italy: Springer-Verlag New York, Inc; 1994:171–182.

Kotsianos-Hermle D, Hiltawsky KM, Wirth S, Fischer T, Friese K, Reiser M. Analysis of 107 breast lesions with automated 3-D ultrasound and comparison with mammography and manual ultrasound. Eur J Radiol 2009;71:109–115.

Leconte I, Feger C, Galant C, Berliere M, Berg BV, D'Hoore W, Maldague B. Mammography and subsequent whole-breast sonography of nonpalpable breast cancers: The importance of radiologic breast density. AJR Am J Roentgenol 2003;180:1675–1679.

Lee JS. Digital image smoothing and the sigma filter. Comput Vision Graph 1983;24:255–269.

Meinel LA, Stolpen AH, Berbaum KS, Fajardo LL, Reinhardt JM. Breast MRI lesion classification: Improved performance of human readers with a backpropagation neural network computer-aided diagnosis (CAD) system. J Magn Reson Imaging 2007;25:89–95.

Mulchrone KF, Choudhury KR. Fitting an ellipse to an arbitrary shape: Implications for strain analysis. J Struct Geol 2004;26:143–153.

Nothacker M, Duda V, Hahn M, Warm M, Degenhardt F, Madjar H, Weinbrenner S, Albert US. Early detection of breast cancer: Benefits and risks of supplemental breast ultrasound in asymptomatic women with mammographically dense breast tissue. A systematic review. BMC Cancer 2009;9:335.

Rahbar G, Sie AC, Hansen GC, Prince JS, Melany ML, Reynolds HE, Jackson VP, Sayre JW, Bassett LW. Benign versus malignant solid breast masses: US differentiation. Radiology 1999;213:889–894.

Sethian JA. Level set methods: Evolving interfaces in geometry, fluid mechanics, computer vision, and materials science. Cambridge: Cambridge University Press; 1996.

Sethian JA. Level set methods and fast marching methods: Evolving interfaces in computational geometry, fluid mechanics, computer vision, and materials science. Cambridge, UK ; New York: Cambridge University Press; 1999.

Shen WC, Chang RF, Moon WK. Computer aided classification system for breast ultrasound based on breast imaging reporting and data system (BI-RADS). Ultrasound Med Biol 2007a;33:1688–1698.

Shen WC, Chang RF, Moon WK, Chou YH, Huang CS. Breast ultrasound computer-aided diagnosis using BI-RADS features. Acad Radiol 2007b;14:928–939.

Stavros AT, Thickman D, Rapp CL, Dennis MA, Parker SH, Sisney GA. Solid breast nodules: Use of sonography to distinguish between benign and malignant lesions. Radiology 1995;196:123–134.

Suri JS, Kathuria C, Chang R-F, Molinari F, Fenster A. Advances in diagnostic and therapeutic ultrasound imaging. Norwood, MA: Artech House; 2008.

Ulanovsky A, Prohl G. A practical method for assessment of dose conversion coefficients for aquatic biota. Radiat Environ Biophys 2006;45:203–214.

Zhu Q, Poh L-K. A transformation-invariant recursive subdivision method for shape analysis. 9th International Conference on Pattern Recognition. Rome, Italy: IEEE; 1988:2:833-835.